ACS NANO
www.acsnano.org
ARTICLE

Competition between Hydrogen Bonds and Coordination Bonds Steered by the Surface Molecular Coverage

Liangliang Cai, Qiang Sun, Meiling Bao, Honghong Ma, Chunxue Yuan, and Wei Xu*

Interdisciplinary Materials Research Center, Tongji-Aarhus Joint Research Center for Nanostructures and Functional Nanomaterials, College of Materials Science and Engineering, Tongji University, Shanghai 201804, P. R. China

S *Supporting Information*

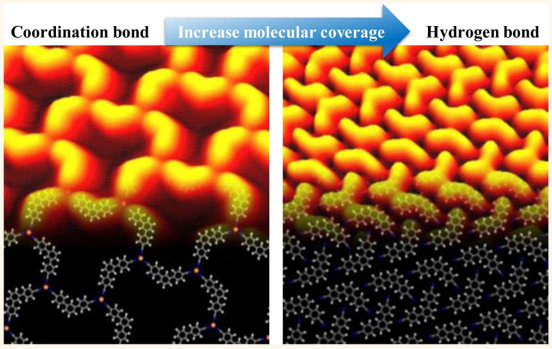

ABSTRACT: **In addition to the choices of metal atoms/molecular linkers and surfaces, several crucial parameters, including surface temperature, molecular stoichiometric ratio, electrical stimulation, concentration, and solvent effect for liquid/solid interfaces, have been demonstrated to play key roles in the formation of on-surface self-assembled supramolecular architectures. Moreover, self-assembled structural transformations frequently occur in response to a delicate control over those parameters, which, in most cases, involve either conversions from relatively weak interactions to stronger ones (e.g., hydrogen bonds to coordination bonds) or transformations between the comparable interactions (e.g., different coordination binding modes or hydrogen bonding configurations). However, intermolecular bond conversions from relatively strong coordination bonds to weak hydrogen bonds were rarely reported. Moreover, to our knowledge, a reversible conversion between hydrogen bonds and coordination bonds has not been demonstrated before. Herein, we have demonstrated a facile strategy for the regulation of stepwise intermolecular bond conversions from the metal−organic coordination bond (Cu−N) to the weak hydrogen bond (CH···N) by increasing the surface molecular coverage. From the DFT calculations we quantify that the loss in intermolecular interaction energy is compensated by the increased molecular adsorption energy at higher molecular coverage. Moreover, we achieved a reversible conversion from the weak hydrogen bond to the coordination bond by decreasing the surface molecular coverage.**

KEYWORDS: *bond conversion, hydrogen bond, metal−organic coordination bond, self-assembly, scanning tunneling microscopy*

In the past two decades, the on-surface bottom-up strategy of supramolecular self-assembly has opened up a promising vista for constructions of highly organized low-dimensional nanostructures with molecular precision and versatile functionalities,[1−11] which bears significant prospects for further applications including heterogeneous catalysis, nanoelectronics, or purely for fundamental science and art.[10−16] The delicate choices of metal atoms/molecular precursors and surfaces are at the heart of constructing desired surface nanostructures. Besides, various parameters, such as substrate temperature,[17−19] concentration,[20−22] molecular stoichiometric ratio if with multicomponents,[23−25] electrical stimulation,[26−28] and solvent effect,[29,30] have been demonstrated to play vital roles in the formation of self-assembled supramolecular architectures, which could also effectively result in diverse structural transformations. For example, Lin et al. achieved the structural transformation by the increment of molecular packing densities in a metal−organic coordination system.[31] Brune et al. regulated the formation of various coordination and hydrogen-bonded structures by adjusting the substrate temperatures.[32] In most of the studies, structural transformations normally involve the change of either coordination binding modes and hydrogen bonding configurations individually or the conversion from relatively weak hydrogen bonds to coordination bonds. However, intermolecular bond conversions from relatively strong coordination bonds to weak hydrogen bonds were rarely reported.[33] Moreover, to the best of our knowledge, a reversible conversion between hydrogen bonds and coordination bonds has not been demonstrated before. It is therefore of particular interest to present a common strategy for the regulation of intermolecular bond conversions with the aim of achieving controllable on-surface molecular self-assemblies.

In this study, we have selected two typical organic molecules with different molecular geometries, but both of the molecules are decorated with carbonitrile end groups which are capable of

Received: December 14, 2016
Accepted: April 6, 2017
Published: April 6, 2017

DOI: 10.1021/acsnano.6b08374
ACS Nano 2017, 11, 3727−3732

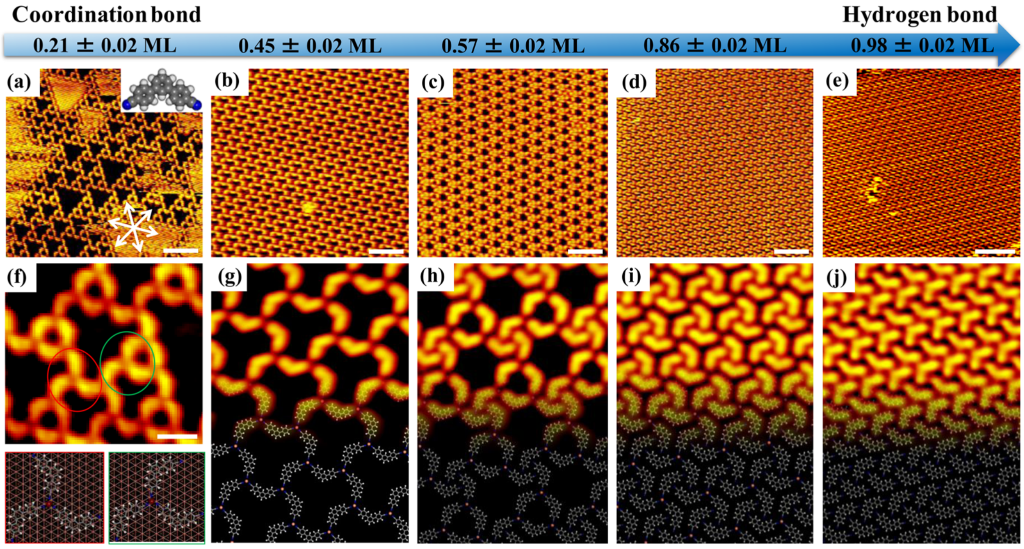

Figure 1. (a) Large-scale and (f) high-resolution STM images showing the formation of metal−organic coordination nanostructures after deposition of TPDCN molecules on the Cu(111) surface (0.21 ± 0.02 ML) at room temperature. Two elementary motifs are indicated by red (i.e., homotactic fan blade structure) and green (i.e., heterotactic one) circles in (f), respectively. Lower panels showing the corresponding DFT optimized models on the surface. Further increasing molecular coverage to (b) 0.45 ± 0.02 ML, (c) 0.57 ± 0.02 ML, (d) 0.86 ± 0.02 ML, and (e) 0.98 ± 0.02 ML via step-by-step depositions of additional TPDCN molecules on the surface at room temperature resulting in the formation of various structures with different binding modes. (b) Homotactic porous network structure, (c) heterotactic porous structure, (d) homotactic windmill structure, and (e) close-packed structure. (g, h, i, j) The corresponding high-resolution STM images with partially superimposed DFT models, respectively. Scale bar in (a−e): 10 nm. Scale bar in (f): 2 nm. White arrows in (a) represent the close-packed directions of the substrate. One ML is defined as 83 TPDCN molecules per 100 nm^2.

coordinating with transition metals as well as forming CH⋯N weak hydrogen bonds.[32,34] As shown in Figure 1a, one molecular precursor named as TPDCN has a 120° V-shaped phenyl backbone, and the other one (shown in Figure 2a) named as BPDCN has a linear backbone. The Cu(111) surface is selected for the sake of providing the copper adatoms and the commensurate substrate symmetry to facilitate the coordination with carbonitrile groups.[12,32] From an interplay of high-resolution scanning tunneling microscopy (STM) imaging and density functional theory (DFT) calculations, we demonstrate that for both TPDCN and BPDCN molecules it is feasible to induce the intermolecular bond conversion from the metal−organic coordination bond (Cu−N) to the weak hydrogen bond (CH⋯N) by a stepwise increase of surface molecular coverage, which consequently results in controllable structural transformations. We quantify that the loss in intermolecular interaction energy is compensated by the increased molecular adsorption energy at higher molecular coverage. Moreover, we achieved a reversible conversion from the weak hydrogen bond to the coordination bond by decreasing the surface molecular coverage.

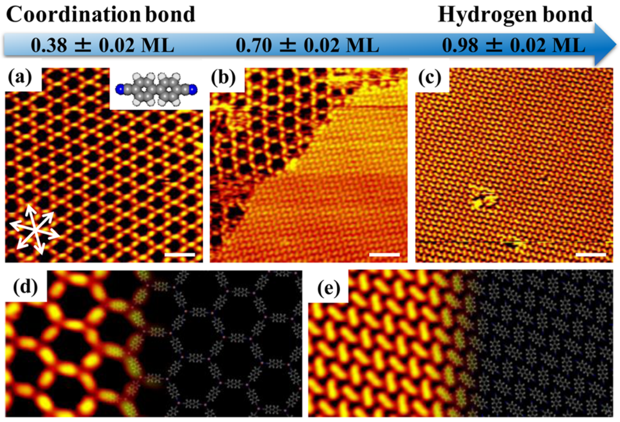

Figure 2. (a) Large-scale STM image showing the metal−organic coordination network after deposition of BPDCN molecules on the Cu(111) surface (0.38 ± 0.02 ML) at room temperature. (b) Large-scale STM image showing the coexistence of the coordination network and the hydrogen-bonded structure after additional deposition of BPDCN molecules to 0.70 ± 0.02 ML at room temperature. (c) Large-scale STM image showing the hydrogen-bonded structure after further increasing the coverage to 0.98 ± 0.02 ML. (d) and (e) showing the high-resolution STM images of the coordination network and the hydrogen-bonded structure with partially superimposed DFT models. (a−c) Scale bar: 7 nm. White arrows in (a) represent the close-packed directions of the substrate. One ML is defined as 118 BPDCN molecules per 100 nm^2.

RESULTS AND DISCUSSION

After deposition of TPDCN molecules step by step on the Cu(111) surface held at room temperature, we obtain a series of different surface nanostructures as shown in Figure 1. Figure 1a shows that deposition of TPDCN molecules at a relatively low coverage of 0.21 ± 0.02 monolayer (ML) results in the formation of porous nanostructures, in which two kinds of elementary coordination motifs are identified as indicated by the red and green circles in the close-up STM image (*cf.* Figure 1f). Both motifs are identified as 3-fold structures, and based on the molecular arrangements they are defined as homotactic (red) and heterotactic (green) fan blade structures, respectively. The heterotactic one is similar to what we reported before (the same molecule coordinated with Ni atoms on the Au(111) surface),[11] which is the elementary motif for construction of molecular Sierpiński triangle. While, in the present case because of the coexistence of homotactic and heterotactic ones, only zero generation Sierpiński triangle can be formed. To get

Table 1. Molecular Coverage, Densities, STM Images of Each Building Block, DFT Relaxed Models of Each Building Block, Cu/Molecule Ratios within Each Building Block, Intermolecular Bonds, Intermolecular Interaction Energy (E_{mol_mol}), Adsorption Energy (E_{mol_sub}), and Total Binding Energy (E_{tb}) on the Cu(111) Substrate of Each Phase Formed by the TPDCN and the BPDCN Molecule, Respectively

Molecules	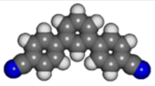 TPDCN				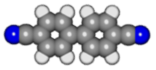 BPDCN	
Coverage (monolayer)	0.45 ± 0.02	0.57 ± 0.02	0.86 ± 0.02	0.98 ± 0.02	0.38 ± 0.02	0.98 ± 0.02
Molecules / 100 nm²	37 ± 2	47 ± 2	71 ± 2	81 ± 2	45 ± 2	116 ± 2
STM images	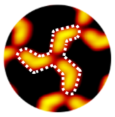	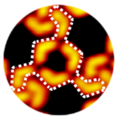	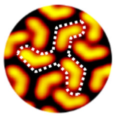	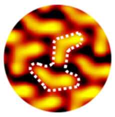	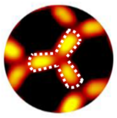	
Building blocks	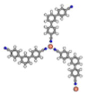	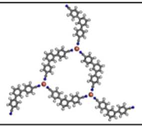	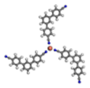	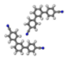	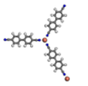	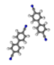
Cu : molecule ratios within each building block	2 : 3	3 : 6	1 : 3	0 : 2	2 : 3	0 : 2
Intermolecular bonds	Coordination bond	Coordination and hydrogen bonds	Coordination and hydrogen bonds	Hydrogen bond	Coordination bond	Hydrogen bond
E_{mol_mol} (eV/molecule)	-1.91	/	/	-0.55	-2.17	-0.39
E_{mol_sub} (eV/molecule)	-1.28	/	/	-2.25	-0.72	-1.62
E_{tb} (eV/100 nm²)	-133.69	/	/	-197.30	-133.26	-174.88

atomic-scale models, DFT calculations are performed on the homotactic and heterotactic structures on Cu(111) as shown in the lower panel of Figure 1f. In both motifs, one copper atom coordinates with three TPDCN molecules and adsorbs at the hollow site of the substrate with a height of 1.09 Å below the molecular plane. Notably, the nitrogen atoms are tilted downward by coordinating with the underlying copper atom, and the bond length of Cu−N is 1.98 Å.

Interestingly, gradual depositions of additional molecules result in a series of structural transformations. Figure 1b is a typical overview STM image of the sample on which the surface coverage is increased to 0.45 ± 0.02 ML where an extended well-organized porous network structure is formed. The close-up STM image (Figure 1g) allows us to distinguish that the porous structure is composed of homotactic fan blade motifs. In combination with the DFT relaxed model superimposed on the high-resolution STM image, we identify that the building block of this phase is composed of three molecules and two copper atoms as depicted in Table 1, and both carbonitrile groups of all the molecules are coordinated with copper atoms. The homotactic porous structure is thus purely linked by coordination bonds.

If we keep on depositing additional molecules with the coverage to 0.57 ± 0.02 ML, we find a structural transformation from the homotactic porous structure to a heterotactic porous one as shown in Figure 1c and h, in which the elementary motif is the heterotactic fan blade one. From the DFT relaxed model, we identify that the building block of this phase is composed of six molecules and three copper atoms as depicted in Table 1, which is defined as a zero generation Sierpiński triangle.[11] It is noteworthy that one of the carbonitrile groups within the heterotactic fan blade motif forms the CH···N hydrogen bond, and the other carbonitrile groups are coordinated with copper atoms. The heterotactic porous structure is then formed by synergistic interactions of coordination bonds and weak hydrogen bonds.

After further increasing the molecular coverage to 0.86 ± 0.02 ML, it is intriguing to form a new windmill structure composed of homotactic fan blade motif again as shown in Figure 1d and i. In combination with the DFT relaxed model, we identify that the building block of this phase is composed of three molecules and one copper atom as depicted in Table 1, and one carbonitrile group of all the molecules forms the coordination bond, and the other carbonitrile group forms the hydrogen bond. The windmill structure is stabilized by a combination of coordination bonds and hydrogen bonds. It is noticed that the cooper atom/molecule ratios are decreased from 2:3 over 3:6 to 1:3 within the formed nanostructures (cf. Table 1), and correspondingly, the contributions of coordination bonds are gradually balanced by the weak hydrogen bonds.

If we keep on depositing additional molecules to 0.98 ± 0.02 ML, surprisingly, we end up with a more compact structure as shown in Figure 1e. The close-up STM image (Figure 1j) and the DFT relaxed model allow us to distinguish that the close-packed structure is composed of hydrogen-bonded dimers as the building block (depicted in Table 1). Now both carbonitrile groups of the molecules form the hydrogen bonds, and the structure is thus purely linked by intermolecular hydrogen bonds, which is in analogy to the self-assembly of carbonitrile functionalized molecules on gold and silver surfaces.[11,34] To verify these unexpected structural transformation processes accompanied by the competition between hydrogen bonds and coordination bonds, we have done control experiments by directly depositing TPDCN molecules on the surface with different coverage (0.45 ± 0.02 ML, 0.57 ± 0.02 ML, 0.86 ± 0.02 ML, and 0.98 ± 0.02 ML), respectively. As expected, we

DOI: 10.1021/acsnano.6b08374

obtain the corresponding structures that are in accordance with the ones obtained by the stepwise deposition manner. Also, deposition of TPDCN molecules at intermediate molecular coverage results in coexistence of different structures as shown in Figure S1. Moreover, we perform further experiments by thermal desorption of molecules from the pure hydrogen bonded structure (0.98 ± 0.02 ML) to lower molecular coverage and readsorption of the molecules back to 0.98 ± 0.02 ML as shown in Figure S2. From such a sequential experiment, we achieve a reversible conversion from the weak hydrogen bond to the coordination bond by decreasing the surface molecular coverage.

To quantify the competition between hydrogen bonds and coordination bonds, also to quantify the cooperative effect of intermolecular interactions and molecule–substrate interactions with different molecular coverage, we have performed a number of calculations including the total binding energy (E_{tb}), the intermolecular interaction energy (E_{mol_mol}), and the adsorption energy (E_{mol_sub}) on the Cu(111) substrate as listed in Table 1. E_{tb} is defined as the total energy of the whole relaxed system (including the formed hydrogen-bonded and/or coordination-bonded molecular structures and the Cu(111) substrate) minus the total energies of all of the individual relaxed components. That is, $E_{tb} = E_{sys} - E_{mol} - E_{sub}$, where E_{sys} represents the total energy of the whole system, E_{mol} represents the total energy of the relaxed molecules, and E_{sub} represents the energy of the relaxed substrate. E_{mol_mol} is defined as the total energy of the whole relaxed structure on the surface minus the energies of each individual components (molecules and/or molecule together with metal adatoms for the pure coordination structures) calculated in the geometry of the corresponding structures. That is, $E_{mol\_mol} = E'_{sys} - E'_{mol} - E'_{ada}$, where E'_{sys} represents the total energy of the whole structure, E'_{mol} and E'_{ada} represent the energies of the molecules and adatoms in the geometry of the corresponding structures, respectively. E_{mol_sub} is defined as the total energy of the system (including the molecule and Cu(111) substrate) minus the energies of the individual molecule and Cu(111) substrate calculated in the geometry of the corresponding structures. That is, $E_{mol\_sub} = E'_{sys} - E'_{mol} - E'_{sub}$, where E'_{sys} represents the total energy of the system, E'_{mol} and E'_{sub} represent the energies of the molecule and Cu(111) substrate in the geometry of the corresponding structures, respectively.

For the TPDCN molecule, E_{tb} of the pure coordination-bonded structure and the pure hydrogen-bonded structure were calculated to be −133.69 eV/100 nm^2 and −197.30 eV/100 nm^2, respectively. E_{mol_mol} of the pure coordination-bonded structure and the pure hydrogen-bonded structure were calculated to be −1.91 eV/molecule and −0.55 eV/molecule, respectively. E_{mol_sub} of the pure coordination-bonded structure and the pure hydrogen-bonded structure were calculated to be −1.28 eV/molecule and −2.25 eV/molecule, respectively. So even though the close-packed structure (Figure 1e) is dominated by the weak CH···N hydrogen bonds, the loss in intermolecular interaction energy with respect to the Cu–N coordination bonds is compensated by the increased molecular adsorption energy at higher molecular coverage. Due to the really large unit cell of the structures at intermediate molecular coverage, we have tried our best, but finally we could not run such calculations at the moment.

To demonstrate the generality of the facile strategy on steering the competition between hydrogen bonds and coordination bonds by the molecular coverage, we choose a linear molecule BPDCN with the same functional groups as TPDCN. After deposition of BPDCN molecules at a relatively low coverage (0.38 ± 0.02 ML) on Cu(111) substrate at room temperature, we observe the formation of the honeycomb network as shown in Figure 2a. From the close-up STM image together with the partially superimposed DFT relaxed models (Figure 2d), we identify that the building block of the coordination network is composed of three BPDCN molecules and two copper atoms as depicted in Table 1.

Then, we deposit additional BPDCN molecules step by step on the coordination-network-covered surface at room temperature, expectedly, we achieve a stepwise structural transformation from the coordination network (0.38 ± 0.02 ML) over the coexistence of coordination and hydrogen-bonded structures (0.70 ± 0.02 ML) to the pure hydrogen-bonded one (0.98 ± 0.02 ML) as shown in Figure 2a–c. In combination with the DFT relaxed model partially superimposed on the close-up STM image (Figure 2e), we identify that the molecules are purely hydrogen-bonded between the carbonitrile groups and phenyl groups (CH···N) within the structure. The building block of the hydrogen-bonded structure is a dimer motif as depicted in Table 1. Moreover, we perform further experiments by thermal desorption of the BPDCN molecules from the pure hydrogen bonded structure (0.98 ± 0.02 ML) to lower molecular coverage as shown in Figure 3. In this process, we achieve a reversible conversion from the weak hydrogen bonded structure to the metal–organic coordination network by decreasing the surface molecular coverage through flashing the sample to 385 K.

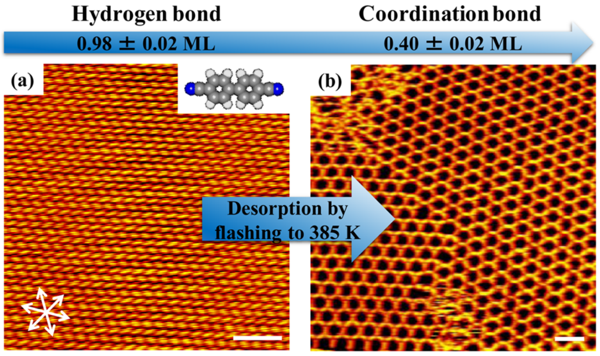

Figure 3. (a) Large-scale STM image showing the hydrogen-bonded structure after deposition of BPDCN molecules on the Cu(111) surface (0.98 ± 0.02 ML) at room temperature. (b) Large-scale STM image showing the metal–organic coordination network after flashing the sample to 385 K. Scale bar: 5 nm. White arrows in (a) represent the close-packed directions of the substrate.

To further quantify the conversion process, we also perform extensive calculations on this system as listed in Table 1. For the BPDCN molecule, the situation is similar to the one of the TPDCN molecule. E_{tb} of the pure coordination-bonded structure and the pure hydrogen-bonded structure were calculated to be −133.26 eV/100 nm^2 and −174.88 eV/100 nm^2, respectively. E_{mol_mol} of the pure coordination-bonded structure and the pure hydrogen-bonded structure were calculated to be −2.17 eV/molecule and −0.39 eV/molecule, respectively. E_{mol_sub} of the pure coordination-bonded structure and the pure hydrogen-bonded structure were calculated to be −0.72 eV/molecule and −1.62 eV/molecule, respectively. Thus, based on the above systematic calculations of two different systems, we conclude that the loss in intermolecular interaction energy is compensated by the increased molecular adsorption energy at higher molecular coverage. The increased molecular adsorption energy at higher molecular coverage originates from two aspects: (i) molecular density and (ii) the increase of molecular adsorption energy (E_{mol_sub}) in the pure hydrogen-bonded structure.

CONCLUSION

In conclusion, by the combination of high-resolution UHV-STM imaging and DFT calculations, we have demonstrated in real space intermolecular bond interconversions between the weak hydrogen bond and the coordination bond steered by the surface molecular coverage. We quantify that the molecular adsorption energy on Cu(111) should be the key to compensating the loss in intermolecular interaction energy at higher molecular coverage. These findings provide a facile method to regulate intermolecular interactions, which may give implications for introducing specific intermolecular bonds for particular applications.

METHODS AND MATERIALS

All the STM experiments were carried out in a UHV chamber with a base pressure of 1×10^{-10} mbar. The whole system was equipped with a SPECS variable-temperature "Aarhus-type" STM,[35,36] a molecular evaporator and standard facilities for sample preparation. The Cu(111) substrate was prepared by several cycles of 1.5 keV Ar^+ sputtering followed by annealing to 850 K, resulting in clean and flat terraces separated by monatomic steps. After the system was thoroughly degassed, the TPDCN (that is, [1,1′: 3′,1″-terphenyl]-4, 4″-dicarbonitrile) and BPDCN (that is, [1,1′-biphenyl]-4,4′-dicarbonitrile) molecules were sublimated from the molecular evaporator onto the Cu(111) substrate. The TPDCN molecule was prepared according to the literature.[37] The chemicals for the synthesis of TPDCN were purchased from Adamas. The BPDCN molecule was purchased from Tokyo Chemical Industry Co., Ltd. with purity >97%. The sample was thereafter transferred within the UHV chamber to the microscope, where measurements were performed in a typical temperature range of 100−150 K, and the typical scanning parameters were: I_t = 0.5−1.0 nA, V_t = ± 1000−2000 mV.

All the calculations were performed in the framework of DFT by using Vienna *Ab Initio* Simulation Package (VASP) code.[38,39] The projector augmented wave method was used to describe the interaction between ions and electrons,[40,41] and the Perdew−Burke−Ernzerh of generalized gradient approximation exchange−correlation functional was employed.[42] van der Waals corrections to the PBE density functional were also included using the DFT-D3 method of Grimme.[43] The atomic structures were relaxed using the conjugate gradient algorithm scheme as implemented in VASP until the forces on all unconstrained atoms were ≤0.03 eV/Å. Plane waves were used as a basis set with an energy cutoff of 400 eV for the models, and calculations were performed on a 2*2*1 k-point grid. For the DFT calculations of the self-assembled structures, due to the large supercell used, the Cu(111) surface was included as a one-layer slab with a total height of 18.0 Å.

ASSOCIATED CONTENT

Supporting Information

The Supporting Information is available free of charge on the ACS Publications website at DOI: 10.1021/acsnano.6b08374.

Additional STM images (PDF)

AUTHOR INFORMATION

Corresponding Author

*xuwei@tongji.edu.cn.

ORCID

Wei Xu: 0000-0003-0216-794X

Notes

The authors declare no competing financial interest.

ACKNOWLEDGMENTS

The authors acknowledge the financial support from the National Natural Science Foundation of China (21473123, 21622307, 51403157).

REFERENCES

(1) Pawin, G.; Wong, K. L.; Kwon, K. Y.; Bartels, L. A Homomolecular Porous Network at a Cu(111) Surface. *Science* **2006**, *313*, 961−962.

(2) Otero, R.; Lukas, M.; Kelly, R. E. A.; Xu, W.; Lægsgaard, E.; Stensgaard, I.; Kantorovich, L. N.; Besenbacher, F. Elementary Structural Motifs in a Random Network of Cytosine Adsorbed on a Gold(111) Surface. *Science* **2008**, *319*, 312−315.

(3) Kong, H.; Zhang, C.; Xie, L.; Wang, L.; Xu, W. Constitutional Dynamics of Metal-Organic Motifs on a Au(111) Surface. *Angew. Chem., Int. Ed.* **2016**, *55*, 7157−7160.

(4) Kepčija, N.; Zhang, Y. Q.; Kleinschrodt, M.; Björk, J.; Klyatskaya, S.; Klappenberger, F.; Ruben, M.; Barth, J. V. Steering On-Surface Self-Assembly of High-Quality Hydrocarbon Networks with Terminal Alkynes. *J. Phys. Chem. C* **2013**, *117*, 3987−3995.

(5) Abdurakhmanova, N.; Floris, A.; Tseng, T. C.; Comisso, A.; Stepanow, S.; De Vita, A.; Kern, K. Stereoselectivity and Electrostatics in Charge-Transfer Mn- and Cs-TCNQ4 Networks on Ag(100). *Nat. Commun.* **2012**, *3*, 940.

(6) Sirtl, T.; Schlögl, S.; Rastgoo-Lahrood, A.; Jelic, J.; Neogi, S.; Schmittel, M.; Heckl, W. M.; Reuter, K.; Lackinger, M. Control of Intermolecular Bonds by Deposition Rates at Room Temperature: Hydrogen Bonds *versus* Metal Coordination in Trinitrile Monolayers. *J. Am. Chem. Soc.* **2013**, *135*, 691−695.

(7) Sun, K.; Shao, T. N.; Xie, J. L.; Lan, M.; Yuan, H. K.; Xiong, Z. H.; Wang, J. Z.; Xue, Q. K.; Liu, Y. Chiral Pinwheel Clusters Lacking Local Point Chirality. *Small* **2012**, *8*, 2078−2082.

(8) Zhang, C.; Xie, L.; Wang, L.; Kong, H.; Tan, Q.; Xu, W. Atomic-Scale Insight into Tautomeric Recognition, Separation and Interconversion of Guanine Molecular Networks on Au(111). *J. Am. Chem. Soc.* **2015**, *137*, 11795−11800.

(9) Stohr, M.; Boz, S.; Schär, M.; Nguyen, M. T.; Pignedoli, C. A.; Passerone, D.; Schweizer, W. B.; Thilgen, C.; Jung, T. A.; Diederich, F. Self-Assembly and Two-Dimensional Spontaneous Resolution of Cyano-Functionalized [7] Helicenes on Cu(111). *Angew. Chem., Int. Ed.* **2011**, *50*, 9982−9986.

(10) Shang, J.; Wang, Y.; Chen, M.; Dai, J.; Zhou, X.; Kuttner, J.; Hilt, G.; Shao, X.; Gottfried, J. M.; Wu, K. Assembling Molecular Sierpiński Triangle Fractals. *Nat. Chem.* **2015**, *7*, 389−393.

(11) Sun, Q.; Cai, L.; Ma, H.; Yuan, C.; Xu, W. On-Surface Construction of a Metal−Organic Sierpiński Triangle. *Chem. Commun.* **2015**, *51*, 14164−14166.

(12) Pivetta, M.; Pacchioni, G. E.; Schlickum, U.; Barth, J. V.; Brune, H. Formation of Fe Cluster Superlattice in a Metal-Organic Quantum-Box Network. *Phys. Rev. Lett.* **2013**, *110*, 086102.

(13) Cheng, Z.; Wyrick, J.; Luo, M.; Sun, D.; Kim, D.; Zhu, Y.; Lu, W.; Kim, K.; Einstein, T. L.; Bartels, L. Adsorbates in a Box: Titration of Substrate Electronic States. *Phys. Rev. Lett.* **2010**, *105*, 066104.

(14) Stepanow, S.; Lingenfelder, M.; Dmitriev, A.; Spillmann, H.; Delvigne, E.; Lin, N.; Deng, X.; Cai, C.; Barth, J. V.; Kern, K. Steering Molecular Organization and Host−Guest Interactions Using Two-Dimensional Nanoporous Coordination Systems. *Nat. Mater.* **2004**, *3*, 229−233.

(15) Grumelli, D.; Wurster, B.; Stepanow, S.; Kern, K. Bio-Inspired Nanocatalysts for the Oxygen Reduction Reaction. *Nat. Commun.* **2013**, *4*, 2904.

(16) Nieckarz, D.; Szabelski, P. Simulation of the Self-Assembly of Simple Molecular Bricks into Sierpiński Triangles. *Chem. Commun.* **2014**, *50*, 6843−6845.

(17) Gutzler, R.; Sirtl, T.; Dienstmaier, J. F.; Mahata, K.; Heckl, W. M.; Schmittel, M.; Lackinger, M. Reversible Phase Transitions in Self-Assembled Monolayers at the Liquid−Solid Interface: Temperature-Controlled Opening and Closing of Nanopores. *J. Am. Chem. Soc.* **2010**, *132*, 5084−5090.

(18) Merz, L.; Parschau, M.; Zoppi, L.; Baldridge, K. K.; Siegel, J. S.; Ernst, K. H. Reversible Phase Transitions in a Buckybowl Monolayer. *Angew. Chem., Int. Ed.* **2009**, *48*, 1966−1969.

(19) Ruben, M.; Payer, D.; Landa, A.; Comisso, A.; Gattinoni, C.; Lin, N.; Collin, J. P.; Sauvage, J. P.; De Vita, A.; Kern, K. 2D Supramolecular Assemblies of Benzene-1,3,5-triyl-tribenzoic Acid: Temperature-Induced Phase Transformations and Hierarchical Organization with Macrocyclic Molecules. *J. Am. Chem. Soc.* **2006**, *128*, 15644−15651.

(20) Tahara, K.; Okuhata, S.; Adisoejoso, J.; Lei, S.; Fujita, T.; Feyter, S. De; Tobe, Y. 2D Networks of Rhombic-Shaped Fused Dehydrobenzo [12] annulenes: Structural Variations under Concentration Control. *J. Am. Chem. Soc.* **2009**, *131*, 17583−17590.

(21) Lei, S.; Tahara, K.; De Schryver, F. C.; Van derAuweraer, M.; Tobe, Y.; De Feyter, S. One Building Block, Two Different Supramolecular Surface-Confined Patterns: Concentration in Control at the Solid−Liquid Interface. *Angew. Chem., Int. Ed.* **2008**, *47*, 2964−2968.

(22) Kampschulte, L.; Werblowsky, T. L.; Kishore, R. S. K.; Schmittel, M.; Heckl, W. M.; Lackinger, M. Thermodynamical Equilibrium of Binary Supramolecular Networks at the Liquid−Solid Interface. *J. Am. Chem. Soc.* **2008**, *130*, 8502−8507.

(23) Huang, Y. L.; Chen, W.; Li, H.; Ma, J.; Pflaum, J.; Wee, A. T. S. Tunable Two-Dimensional Binary Molecular Networks. *Small* **2010**, *6*, 70−75.

(24) Wakayama, Y.; de Oteyza, D. G.; Garcia-Lastra, J. M.; Mowbray, D. J. Solid-State Reactions in Binary Molecular Assemblies of F_{16}CuPc and Pentacene. *ACS Nano* **2011**, *5*, 581−589.

(25) Treier, M.; Nguyen, M. T.; Richardson, N. V.; Pignedoli, C.; Passerone, D.; Fasel, R. Tailoring Low-Dimensional Organic Semiconductor Nanostructures. *Nano Lett.* **2009**, *9*, 126−131.

(26) Mali, K. S.; Wu, D.; Feng, X.; Müllen, K.; Van der Auweraer, M.; De Feyter, S. Scanning Tunneling Microscopy-Induced Reversible Phase Transformation in the Two-Dimensional Crystal of a Positively Charged Discotic Polycyclic Aromatic Hydrocarbon. *J. Am. Chem. Soc.* **2011**, *133*, 5686−5688.

(27) Kong, H.; Wang, L.; Sun, Q.; Zhang, C.; Tan, Q.; Xu, W. Controllable Scission and Seamless Stitching of Metal-Organic Clusters by STM Manipulation. *Angew. Chem., Int. Ed.* **2015**, *54*, 6526−6530.

(28) Yanagi, H.; Ikuta, K.; Mukai, H.; Shibutani, T. STM-Induced Flip-Flop Switching of Adsorbed Subphthalocyanine Molecular Arrays. *Nano Lett.* **2002**, *2*, 951−955.

(29) Mamdouh, W.; Uji-i, H.; Ladislaw, J. S.; Dulcey, A. E.; Percec, V.; De Schryver, F. C.; De Feyter, S. Solvent Controlled Self-Assembly at the Liquid-Solid Interface Revealed by STM. *J. Am. Chem. Soc.* **2006**, *128*, 317−325.

(30) Tahara, K.; Furukawa, S.; Uji-i, H.; Uchino, T.; Ichikawa, T.; Zhang, J.; Mamdouh, W.; Sonoda, M.; De Schryver, F. C.; De Feyter, S.; Tobe, Y. Two-Dimensional Porous Molecular Networks of Dehydrobenzo [12] annulene Derivatives *via* Alkyl Chain Interdigitation. *J. Am. Chem. Soc.* **2006**, *128*, 16613−16625.

(31) Liu, J.; Lin, T.; Shi, Z.; Xia, F.; Dong, L.; Liu, P. N.; Lin, N. Structural Transformation of Two-Dimensional Metal-Organic Coordination Networks Driven by Intrinsic In-Plane Compression. *J. Am. Chem. Soc.* **2011**, *133*, 18760−18766.

(32) Pivetta, M.; Pacchioni, G. E.; Fernandes, E.; Brune, H. Temperature-Dependent Self-Assembly of NC−Ph5−CN Molecules on Cu(111). *J. Chem. Phys.* **2015**, *142*, 101928.

(33) Wang, Y.; Fabris, S.; White, T. W.; Pagliuca, F.; Moras, P.; Papagno, M.; Topwal, D.; Sheverdyaeva, P.; Carbone, C.; Lingenfelder, M.; Classen, T.; Kern, K.; Costantini, G. Varying Molecular Interactions by Coverage in Supramolecular Surface Chemistry. *Chem. Commun.* **2012**, *48*, 534−536.

(34) Schlickum, U.; Decker, R.; Klappenberger, F.; Zoppellaro, G.; Klyatskaya, S.; Auwärter, W.; Neppl, S.; Kern, K.; Brune, H.; Ruben, M.; Barth, J. V. Chiral Kagomé Lattice from Simple Ditopic Molecular Bricks. *J. Am. Chem. Soc.* **2008**, *130*, 11778−11782.

(35) Besenbacher, F. Scanning Tunnelling Microscopy Studies of Metal Surfaces. *Rep. Prog. Phys.* **1996**, *59*, 1737−1802.

(36) Laegsgaard, E.; Österlund, L.; Thostrup, P.; Rasmussen, P. B.; Stensgaard, I.; Besenbacher, F. A High-Pressure Scanning Tunneling Microscope. *Rev. Sci. Instrum.* **2001**, *72*, 3537−3542.

(37) Patrick, D. A.; Ismail, M. A.; Arafa, R. K.; Wenzler, T.; Zhu, X.; Pandharkar, T.; Jones, S. K.; Werbovetz, K. A.; Brun, R.; Boykin, D. W.; Tidwell, R. R. Synthesis and Antiprotozoal Activity of Dicationic m-Terphenyl and 1,3-Dipyridylbenzene Derivatives. *J. Med. Chem.* **2013**, *56*, 5473−5494.

(38) Kresse, G.; Hafner, J. *Ab Initio* Molecular Dynamics for Open-Shell Transition Metals. *Phys. Rev. B: Condens. Matter Mater. Phys.* **1993**, *48*, 13115−13118.

(39) Kresse, G.; Furthmüller, J. Efficient Iterative Schemes for *Ab Initio* Total-Energy Calculations Using a Plane-Wave Basis Set. *Phys. Rev. B: Condens. Matter Mater. Phys.* **1996**, *54*, 11169−11186.

(40) Blöchl, P. E. Projector Augmented-Wave Method. *Phys. Rev. B: Condens. Matter Mater. Phys.* **1994**, *50*, 17953−17979.

(41) Kresse, G.; Joubert, D. From Ultrasoft Pseudopotentials to the Projector Augmented-Wave Method. *Phys. Rev. B: Condens. Matter Mater. Phys.* **1999**, *59*, 1758−1775.

(42) Perdew, J. P.; Burke, K.; Ernzerhof, M. Generalized Gradient Approximation Made Simple. *Phys. Rev. Lett.* **1996**, *77*, 3865−3868.

(43) Grimme, S.; Antony, J.; Ehrlich, S.; Krieg, H. A Consistent and Accurate *Ab Initio* Parametrization of Density Functional Dispersion Correction (DFT-D) for the 94 Elements H-Pu. *J. Chem. Phys.* **2010**, *132*, 154104.